Effect of overlap on spreading dynamics on multiplex networks

Huan Wang[1], Chuang Ma[1], Hanshuang Chen[2] and Haifeng Zhang[1]

[1] School of Mathematical Science, Anhui University, Hefei 230601, People's Republic of China
[2] School of Physics and Materials Science, Anhui University, Hefei 230601, People's Republic of China

E-mail: chenhshf@ahu.edu.cn and haifengzhang1978@gmail.com

Abstract. In spite of the attention the study of epidemic dynamics on single-layer networks has received, the epidemic dynamics on multiplex networks is still limited and is facing many challenges. In this work, we consider the susceptible-infected-susceptible-type (SIS) epidemic model on multiplex networks and investigate the effect of overlap among layers on the spreading dynamics. To do so, we assume that the prerequisite of one S-node to be infected is that there is at least one infectious neighbor in each layer. A remarkable result is that the overlap can alter the nature of the phase transition for the onset of epidemic outbreak. Specifically speaking, the system undergoes a usual continuous phase transition when two layers are completely overlapped. Otherwise, a discontinuous phase transition is observed, accompanied by the occurrence of a bistable region in which a disease-free phase and an endemic phase are coexisting. As the degree of the overlap decreases, the bistable region is enlarged. The results are validated by both simulation and mean-field theory.

J. Stat. Mech. (2020) 043402

Contents

1. Introduction

In the past few decades, complex networks have proved to be a powerful framework to characterize the interaction among the constituents of a variety of complex systems, examples range from the social to technological, biological, and other systems in real world [1]. Up to now, are a large number of works paid their attention to the study of the structures of complex networks and the dynamical behaviors taking place on them [2–7]. However, most of these existing achievements mainly focus on single-layer networks. In fact, many real-world complex systems are usually composed of multilayer networks [8, 9]. A multilayer network is a general concept, which includes interdependent networks, interconnected networks, multiplex networks, network of network, and so forth. For example, an interdependent network is formed by the power and communication infrastructures, and the transportation system including a set of locations which is connected by roads, railways, waterways, or airline connections. It has been recognized that the multilayer networks can present some novel features different from the single-layer networks, such as complexity, diversity and fragility [10–14]. The research on multilayer networks has covered a variety of dynamics including evolutionary games [15–17], synchronization [18–20], opinion formation [21, 22], transportation [23, 24], and super-diffusive behavior [13, 25, 26].

Epidemic spreading, such as the susceptible-infected-susceptible (SIS) model, is not only a paradigm for studying non-equilibrium phase transitions, but also has wide applications in real epidemics, computer viruses, rumor spreading, or signal propagation in neural networks [27]. Therefore, the study of epidemic spreading on networks is always one of the most active areas in network science [28]. Recently, with the study in depth of multilayer networks, epidemic spreading on multilayer networks has also attracted

some attention [29–31]. Cozzo *et al* [32] have shown that the epidemic threshold for the SIS model in a multilayer network is always lower than that in any isolated network. Using an individual-based mean-field approach, Wang *et al* [33] further showed that the epidemic threshold can be reduced dramatically if two nodes corresponding to dominant eigenvector components of the adjacency matrices of isolated networks are connected. Similar results were also obtained by a degree-based mean-field approach [34]. However, Dickison *et al* [35] unveiled, based on the percolation theory [36], one important difference between the susceptible-infected-recovered (SIR) model and the SIS model when the coupling between layers is weak enough. Spreading processes in structured metapopulations can be well characterized within the framework of multilayer networks as well [37–39]. de Arruda *et al* [40] used a tensorial representation [41] to derive analytical expressions for the epidemic threshold of the SIS and SIR model on multilayer networks. They showed, on the one hand, the existence of disease localization [42] and the emergence of two or more susceptibility peaks. On the other hand, they found that, when the layer with the lowest eigenvalue is located at the center of multiplex networks, it can effectively act as a barrier to the disease.

A multiplex network is a special type of multilayer network, where the links at each layer represent a different type of interaction between the same set of nodes. One typical example of the multiplex network is social networks, where nodes represent individuals and the different layers correspond to different types of relationship, such as family, friendships, and work-related. A multiplex network also provides a convenient framework for studying the interplay between different dynamical processes [43, 44], including the competing spreading process of epidemic and awareness [45, 46], the cooperative effect among different spreading dynamics [47], and the interplay of spreading dynamics and stochastic migration among different layers [48, 49].

Very recently, discontinuous phase transition of the spreading model on multiplex networks has received growing attention. Velásquez-Rojas and Vazquez [50] coupled contact process for disease spreading with the voter model for opinion formation taking place on two layers of networks, and they showed that a continuous transition in the contact process becomes discontinuous as the infection probability increases beyond a threshold. Pires *et al* [51] proposed an SIS-like model with an extra vaccinated state, in which individuals vaccinate with a probability proportional to their opinions. Meanwhile, individuals update their opinions in terms of peer influence. They also observed a first-order active-absorbing phase transition in the model. Jiang and Zhou [52] studied the effect of resource amount on epidemic control in a modified SIS model on a two-layer network, and they found that the spreading process goes through a first-order phase transition if the infection strength between layers is weak. Su *et al* [53] proposed a reversible social contagion model of community networks that includes the factor of social reinforcement. They showed that the model exhibits a first-order phase transition in the spreading dynamics, and that a hysteresis loop emerges in the system when there is a variety of initially adopted seeds. Chen *et al* [54] studied the dynamics of the SIS model in social-contact multiplex networks when the recovery of infected nodes depends on resources from healthy neighbors in the social layer. They found that as the infection rate increases the infected density varies smoothly from zero to a finite small value and then suddenly jumps to a high value, where a hysteresis phenomenon was also observed.

As mentioned in the last paragraph, most of the reports on discontinuous phase transitions in spread models were mainly caused by the coupling between different dynamics across layers. A natural question arises: whether such a discontinuous phase transition appears in a single spreading model on multiplex networks? To the end, in this work we want to explore a novel discontinuous phase transition in the SIS model. We propose a variant of the SIS model on multiplex networks in which a susceptible individual can be infected only when s(he) has at least one infectious neighbor in each layer. It is obviously that the model incorporates a non-additive characteristic of spread dynamics in multiplex networks. As we shall show later, such a nonlinear effect in inter-layer interactions can induce a discontinuous phase transition for the onset of epidemic outbreak. It is also known that if the spreading dynamics is only a simple superposition of those in each layer, a usual continuous phase transition was observed [32, 40]. Moreover, our model is motivated by some real-world situations. For example, in a rumor spreading process, a piece of false news is likely to be accepted by a person if it was shared simultaneously by multiple types of relationships, such as family members, friends, and coworkers. A person may be prone to purchase a new commodity when (s)he receives recommendations unanimously from friends of different online shopping sites [55]. The main findings of the present work is summarized as follows. A key factor to the nature of phase transition is the degree of edge overlap among different layers. In particular, when the edges in different layers are totally overlapping, the model presents a usual continuous phase transition as the SIS model taking place on the single-layer networks. Interestingly, when the edges are not totally overlapping, the model shows a novel discontinuous phase transition, accompanied by the emergence of the bistable region where the endemic extinction phase and the endemic spread phase are coexisting. The lower degree of overlap, the wider the bistable region is. We also develop a mean-field theory to validate the correctness of the results.

2. Model and simulation details

We consider a spreading model on multiplex networks with two layers, in which each layer contains the same number N of nodes and there exists a one-to-one correspondence between nodes in different layers. The topology in each layer is described by an adjacency matrix $\mathbf{A}^\ell$ ($\ell = 1, 2$), whose entries A_{ij}^ℓ are defined as $A_{ij}^\ell = 1$ if there is an edge from node j to node i in the ℓth layer, and $A_{ij}^\ell = 0$ otherwise. Note that the topology at each layer may be different. For simplicity, we consider connectivity in each layer is symmetric, $A_{ij}^\ell = A_{ji}^\ell$, $\forall i, j$, and the numbers of edges in two layers are the same, $M = \sum_{i<j} A_{ij}^1 = \sum_{i<j} A_{ij}^2$. We define the fraction of overlapping edges on two layers as [56],

$$\mathcal{O} = \frac{\sum_{i<j} A_{ij}^1 A_{ij}^2}{M}, \tag{1}$$

with $0 \leqslant \mathcal{O} \leqslant 1$. For $\mathcal{O} = 0$, there is no overlapping edge in two layers, and for $\mathcal{O} = 1$, the topologies in two layers are exactly the same. To generate a duplex network with a given $\mathcal{O}$, we first produce two identical networks as the first layer and the second layer,

respectively. Then, we fix the first layer unchanged and rewire the edges in the second layer. The rewiring process is described as follows [57]. The first step is to randomly choose an overlapping edge in the two layers. The second step is to break the edge and then to randomly generate a new edge in the second layer, in which we ensures that the new edge in the second layer does not overlap with the first layer. Repeat this process many times until a given value of $\mathcal{O}$ is reached.

We consider an SIS-type spreading dynamics on duplex networks. Each node is either susceptible ($\sigma_i(t) = 0$) or infected ($\sigma_i(t) = 1$) at time t. The dynamics of the model is defined as follows. (i) *Infection*: for a susceptible node i, (s)he can be infected only if there are at least one infectious neighbor in each layer. Denoting by $n_i^\ell = \sum_j A_{ij}^l \sigma_j$ the number of infectious neighbors of node i in the ℓth layer, the rate of node i being infected at time t can be written as

$$R_{\inf} = \lambda \left(\frac{n_i^1 + n_i^2}{2} \right) \Theta \left(n_i^1 - 1 \right) \Theta \left(n_i^2 - 1 \right), \tag{2}$$

where λ is the infection rate, and $\Theta(x)$ is the Heaviside function defined as $\Theta(x) = 1$ for $x \geqslant 0$ and $\Theta(x) = 0$ for $x < 0$. The Heaviside function in equation (2) renders that the total spreading rate is not a simple superposition of the spreading rates in two layers. As mentioned before, we have shown that the setting of equation (2) incorporates some practical considerations observed in real situations, such as rumor spread and commodity recommendations, which highlights the importance of social reinforcement in the spreading of information [58]. We should also note that the spreading dynamics in our model is similar to the threshold model [59] and core spreading model [60, 61] in single-layer networks. (ii) *Recovery*: for an infectious node i, (s)he becomes spontaneously susceptible at time t with a recovery rate μ. Without loss of generality, we set to $\mu = 1$ and define $\beta = \lambda/\mu$ as a dimensionless infection rate. A schematic of our model is shown in figure 1.

We adopt a random sequential-update algorithm to simulate the model [62]. We discretize the time in small time steps Δt. A node i is first chosen randomly and is tried to update its state. If node i is susceptible, (s)he becomes infected with the probability $R_{\inf}\Delta t$. If node i is infected, (s)he recovers to be susceptible with the probability $\mu\Delta t$. Time is then incremented by $\Delta t/N$ and we iterate up to some final time. The selection of Δt is delicate. Too small Δt will lead to the occurrence of null events very frequently, so that the simulation becomes inefficient. Too large Δt will cause the updating probabilities larger than one that are unphysical. In practice, we used $\Delta t = 1/(k_{\max}\lambda)$ to minimize the probability that nothing happens while keeping all probabilities smaller than one, where $k_{\max}$ is the maximal degree of nodes in two layers. Note that the random sequential-update algorithm has been widely used to simulate the continuous-time Markov process. It has also been verified that this algorithm did not produce essential difference from more sophisticated, but computationally demanding, exact Gillespie algorithm [63].
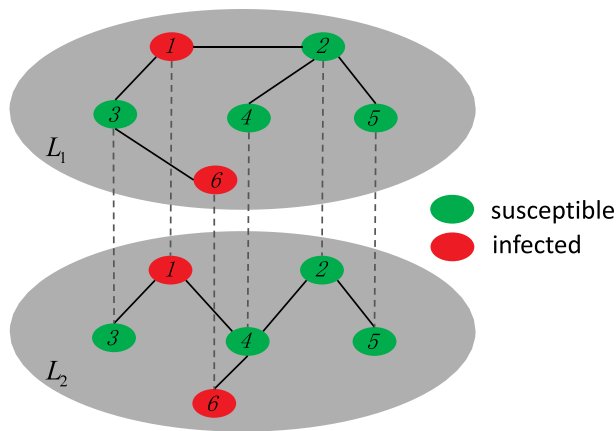
Figure 1. A schematic of our model. A susceptible node can be infected only if there are at least one infected neighbor in each layer, and an infected node can spontaneously recover to be susceptible. According to equation (2), node 3 can be infected by the common infected neighbor (node 1) with the rate 1.5λ. But node 4 cannot be infected as (s)he has no infectious neighbors in the first layer.

3. Simulation results

We first consider the case where two layer networks are consisted of Poisson random graphs [64] with $N = 10\,000$ nodes and the same average degree $\langle k \rangle = 20$. Figure 2 shows the simulation results with two different initial infection density $\rho_0 = 0.02$ and $\rho_0 = 0.98$ and several different values of $\mathcal{O}$, where we have defined $\rho(t) = N^{-1} \sum_{i=1}^{N} \sigma_i(t)$. For $\mathcal{O} = 1$, our model recovers to the usual SIS model in single-layer networks, and the system undergoes a continuous second-order phase transition from a healthy phase to an endemic phase as β increases, separated by a threshold value of β_c (see figure 2(a)). Strikingly, the nature of phase transition is essentially changed to be discontinuous for $\mathcal{O} < 1$, as shown in figures 2(b)–(d). The results for different initial conditions do not coincide in a certain range of $\beta \in [\beta_F, \beta_C]$, forming a hysteresis region that is a typical characteristic of a first-order phase transition. Within the hysteresis region, the system is bistable. Specially, when the initial density of infection is low, the epidemic will become extinct. While for high initial density of infection, the system will maintain a certain proportion of prevalence. As $\mathcal{O}$ decreases, β_F is almost unchanged and β_C shifts to a larger value, thus the bistable region is enlarged.

In figure 3, we show ρ as a function of β in a two-layer network, in which the first layer is a Barabási–Albert (BA) network [65] and the second one is obtained by rewiring edges from a BA network the same as the first layer. The qualitative results are the same as figure 2. That is to say, for a more degree-heterogeneous network we also observe the discontinuous phase transition for the onset of epidemic outbreak and a bistable region with the coexisting healthy phase and endemic phase in a more degree-heterogeneous network. However, to observe such phenomena explicitly, we need to use lower degrees of overlap in edges among layers.

We now consider the case when the number of edges in the two layers are not the same. A particular example of interest is that one layer is completely embedded in
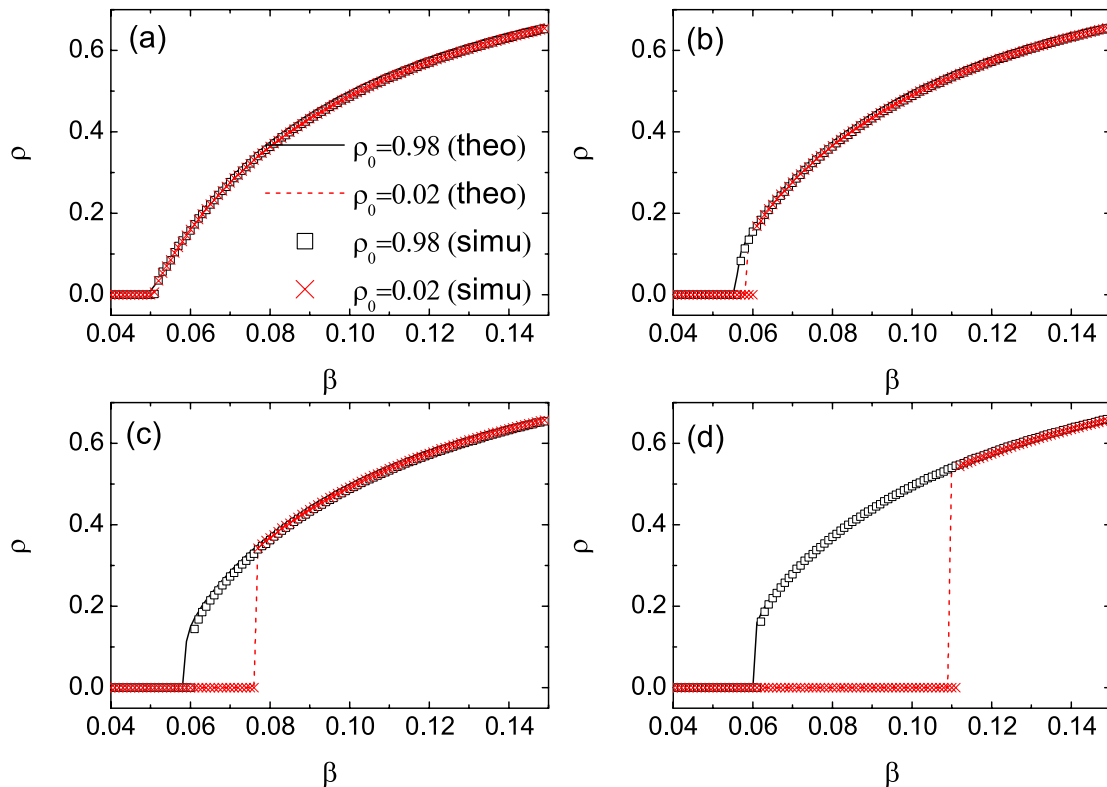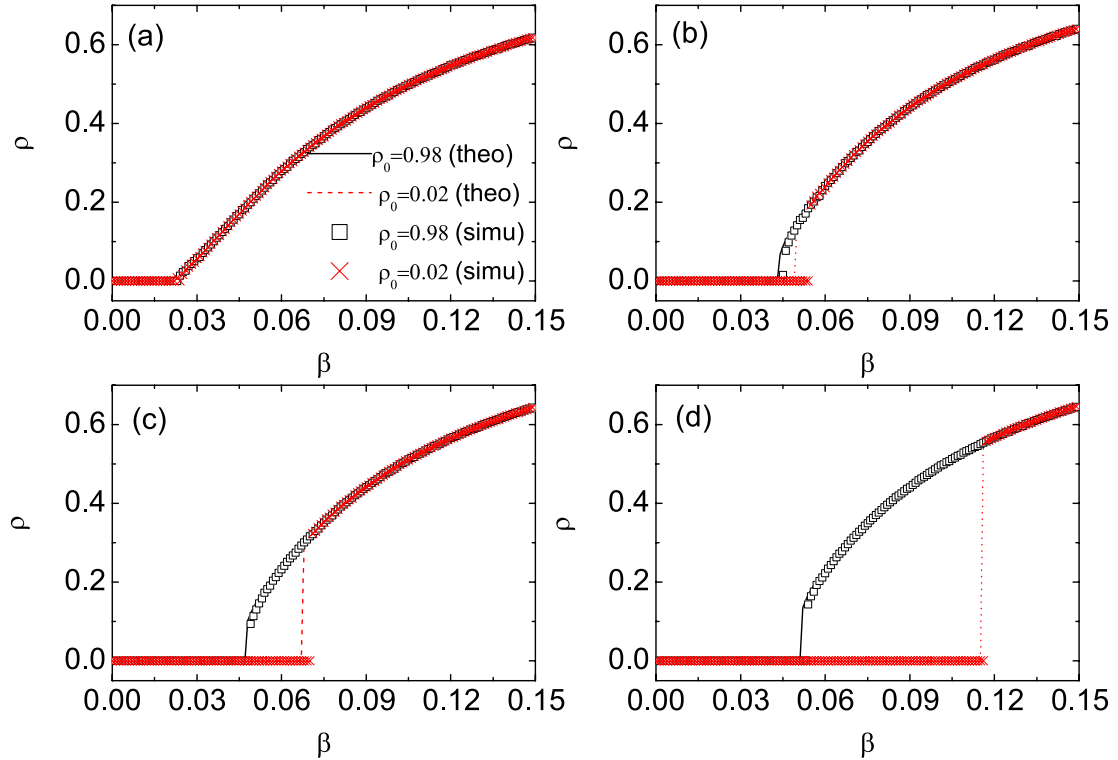
Figure 2. The density of infected nodes ρ as a function of the infection rate β in a two-layer network consisted of two Poisson random graphs. Two different initial infection densities are used: $\rho_0 = 0.98$ (squares) and $\rho_0 = 0.02$ (crosses). From (a) to (d) the overlap parameter $\mathcal{O}$ are 1.0, 0.8, 0.5, and 0.2, respectively. The other parameters are $N = 10\,000$ and $\langle k \rangle = 20$. The lines denote the results of homogeneous mean-field theory (see equation (18)).

another layer. This architecture will yield one layer completely overlapping with the second one but not the vice versa. In figure 4, we show the results in two Poisson random graphs with $N = 10\,000$ nodes. The average degree in the first layer is fixed at 20, and the average degree in the second layer is twice (a) and four times (b) larger than that of the first layer. One can see that the phase transition is discontinuous. If the difference of connection densities between the two layers becomes larger, the discontinuous characteristic of the phase transition will become more obvious.

The key of the discontinuous phase transitions lies in the coexistence of two or more different stable phases. The origin of such a discontinuity in our model stems from the interaction between the nonlinearity of spreading dynamics introducing by equation (2) and the overlapping among the layers. For a multi-layer network with low overlap, an intuitive argument with regard to the coexistence of healthy phase and endemic phase may be presented as follows. For a high initial density of the infected nodes, most of the nodes have at least one infected neighbor in each layer, such that the spread of epidemic is equivalent to that in a single-layer network. When the initial density of the infected nodes is low, the reason why epidemics cannot spread is that most of nodes do not meet the condition of spreading dynamics in equation (2). That is to say, under the latter case, nonlinear effect of spreading dynamics does react and destroy connected

Figure 3. The density of infected nodes ρ as a function of the infection rate β in a two-layer network, in which the first layer is a BA network and the second one is obtained by rewiring edges from a BA network same as the first layer. Two different initial infection densities are used: $\rho_0 = 0.98$ (squares) and $\rho_0 = 0.02$ (crosses). From (a) to (d) the overlap parameter $\mathcal{O}$ are 1.0, 0.2, 0.1, and 0.0, respectively. The other parameters are $N = 10\,000$ and $\langle k \rangle = 20$. The lines denote the results of individual-based mean-field theory (see equation (13)).

infectious clusters, such that the epidemic dies out. This is akin to explosive synchronization in multiplex networks [66, 67], which demonstrate discontinuous transition in one layer due to the suppression of formation of giant cluster drawn from the second layer, either due to frequency mismatch in the mirror nodes [66] or due to negative intralayer coupling of the second layer [67]. In the next section, we will present a formulistic interpretation to the discontinuous phase transition based on a mean-field theory.

4. Mean-field theory

4.1. Individual-based mean-field theory

To be first, let $\rho_i(t)$ denote the probability of node i being infected at time t. That is to say, at time t the state of node i takes the value $\sigma_i(t) = 1$ with the probability $\rho_i(t)$ and $\sigma_i(t) = 0$ with the complementary probability $1 - \rho_i(t)$. To write down the time-evolution equation for node i, a key step is to derive the rate of node i being infected at time t. To do so, we denote by $N_1(i)$ and $N_2(i)$ the set of neighbors of node i in the first
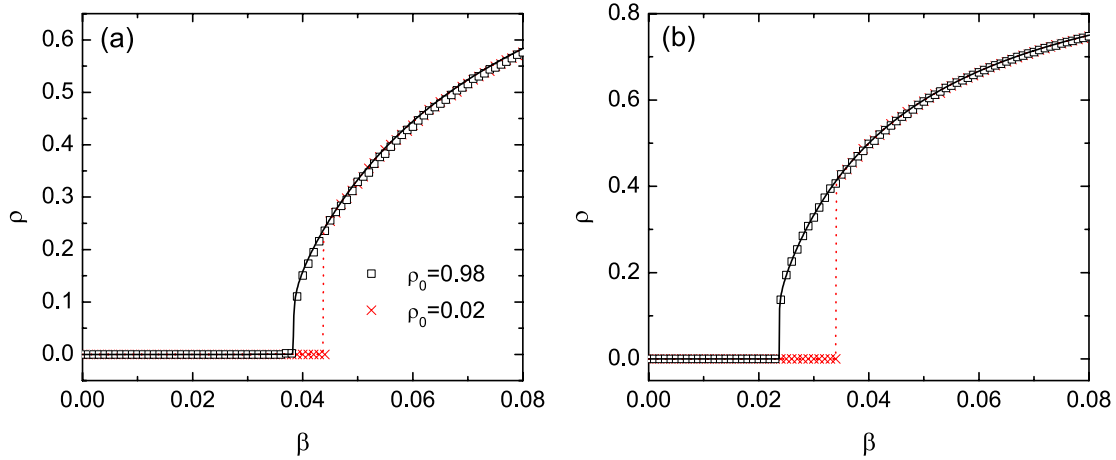
Figure 4. The density of infected nodes ρ as a function of the infection rate β in a two-layer Poisson random graph, in which the first layer is completely overlapped with the second one but not the vice versa. The average degree in the first layer is fixed at 20, and the average degree in the second layer is twice (a) and four times (b) larger than that of the first layer. Two different initial infection densities are used: $\rho_0 = 0.98$ (squares) and $\rho_0 = 0.02$ (crosses). The other parameter is $N = 10\,000$. The lines denote the results of homogeneous mean-field theory (see equation (17)).

layer and in the second layer, respectively. Let $N_\cap(i) = N_1(i) \cap N_2(i)$ denote the set of common neighbors of node i in the two layers, such that $N_{1(2)}(i) = N_\cap(i) + N_{1(2)\backslash\cap}(i)$, where $N_{1(2)\backslash\cap}(i)$ is the set of neighbors of node i belonging to the first (second) layer but not to the second (first) layer, see figure 5 for a schematic. The probability of having $\{n_1, n_2, n_3\}$ infected neighbors out of the sets $N_{1\backslash\cap}(i)$, $N_\cap(i)$, and $N_{2\backslash\cap}(i)$ can be repressed as the product of three Poisson binomial distributions,

$$P(n_1, n_2, n_3) = P_1(n_1) P_2(n_2) P_3(n_3),\tag{3}$$

where

$$P_1(n_1) = \sum_{Z \in F_1} \prod_{j \in Z} \rho_j \prod_{j \in Z^c} (1 - \rho_j).\tag{4}$$

Here F_1 are all the subsets of $N_{1\backslash\cap}(i)$ containing n_1 elements, and Z^c is the complement of Z, i.e. $Z^c = N_{1\backslash\cap}(i)\backslash Z$. Similarly, we can write down the expressions of $P_2(n_2)$ and $P_3(n_3)$, which are not shown here to avoid the duplication. According to equation (2), the rate of node i being infected at time t can be written as,

$$R_{\text{inf}} = \sum_{n_1=0}^{\left|N_{1\backslash\cap}(i)\right|} \sum_{n_2=0}^{\left|N_\cap(i)\right|} \sum_{n_3=0}^{\left|N_{2\backslash\cap}(i)\right|} P(n_1, n_2, n_3) \lambda \left(\frac{n_1 + 2n_2 + n_3}{2}\right) \Theta(n_1 + n_2 - 1) \Theta(n_2 + n_3 - 1),\tag{5}$$

where $\left|N_{1\backslash\cap}(i)\right|$, $\left|N_\cap(i)\right|$, and $\left|N_{2\backslash\cap}(i)\right|$ are the sizes of the sets of $N_{1\backslash\cap}(i)$, $N_\cap(i)$, and $N_{2\backslash\cap}(i)$, respectively. To facilitate the calculation of R_{inf}, we rewrite equation (5) as,
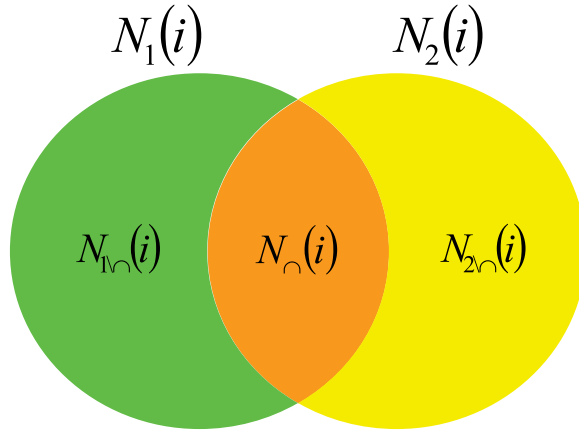
Figure 5. A schematic representation of neighborhood of node i. $N_1(i)$ and $N_2(i)$ denote the sets of neighbors of node i in the first layer and in the second layer, respectively. $N_\cap(i) = N_1(i) \cap N_2(i)$ is the set of common neighbors of node i in the two layers. $N_{1(2)\setminus\cap}(i) = N_{1(2)}(i) - N_\cap(i)$ is the set of neighbors of node i belonging to the first (second) layer but not to the second (first) layer.

$$R_{\text{inf}} = \sum_{n_1=0}^{\left|N_{1\setminus\cap}(i)\right|} \sum_{n_2=0}^{\left|N_\cap(i)\right|} \sum_{n_3=0}^{\left|N_{2\setminus\cap}(i)\right|} P(n_1, n_2, n_3) \lambda \left(\frac{n_1 + 2n_2 + n_3}{2}\right) - \sum_{n_1=0}^{\left|N_{1\setminus\cap}(i)\right|} P(n_1, 0, 0) \lambda \frac{n_1}{2}$$
$$- \sum_{n_3=0}^{\left|N_{2\setminus\cap}(i)\right|} P(0, 0, n_3) \lambda \frac{n_3}{2}. \tag{6}$$

The first term on the right-hand side of equation (6) can be computed as,

$$\sum_{n_1=0}^{\left|N_{1\setminus\cap}(i)\right|} \sum_{n_2=0}^{\left|N_\cap(i)\right|} \sum_{n_3=0}^{\left|N_{2\setminus\cap}(i)\right|} P(n_1, n_2, n_3) \lambda \left(\frac{n_1 + 2n_2 + n_3}{2}\right)$$
$$= \frac{\lambda}{2} \left[\sum_{n_1=0}^{\left|N_{1\setminus\cap}(i)\right|} n_1 P_1(n_1) + \sum_{n_2=0}^{\left|N_\cap(i)\right|} 2n_2 P_2(n_2) + \sum_{n_3=0}^{\left|N_{2\setminus\cap}(i)\right|} n_3 P_3(n_3)\right]$$
$$= \frac{\lambda}{2} \left[\langle n_1 \rangle + 2\langle n_2 \rangle + \langle n_3 \rangle\right], \tag{7}$$

where

$$\langle n_1 \rangle = \sum_{j \in N_{1\setminus\cap}} \rho_j = \sum_j A_{ij}^1 \left(1 - A_{ij}^2\right) \rho_j,$$
$$\langle n_2 \rangle = \sum_{j \in N_\cap} \rho_j = \sum_j A_{ij}^1 A_{ij}^2 \rho_j, \tag{8}$$
$$\langle n_3 \rangle = \sum_{j \in N_{2\setminus\cap}} \rho_j = \sum_j A_{ij}^2 \left(1 - A_{ij}^1\right) \rho_j.$$

The second term and the third term on the right-hand side of equation (6) can be computed as,

$$\sum_{n_1=0}^{\left|N_{1\setminus\cap}(i)\right|} P(n_1,0,0)\,\lambda\frac{n_1}{2} = \frac{\lambda}{2}P_2(0)P_3(0)\sum_{n_1=0}^{\left|N_{1\setminus\cap}(i)\right|} n_1 P_1(n_1) = \frac{\lambda}{2}P_2(0)P_3(0)\langle n_1\rangle,$$

(9)

and

$$\sum_{n_3=0}^{\left|N_{2\setminus\cap}(i)\right|} P(0,0,n_3)\,\lambda\frac{n_3}{2} = \frac{\lambda}{2}P_1(0)P_2(0)\sum_{n_3=0}^{\left|N_{2\setminus\cap}(i)\right|} n_3 P_3(n_3) = \frac{\lambda}{2}P_1(0)P_2(0)\langle n_3\rangle,$$

(10)

respectively. Here

$$P_1(0)P_2(0) = \prod_{j\in N_1(i)}(1-\rho_j) = \prod_j\left(1-A_{ij}^1\rho_j\right),$$

$$P_2(0)P_3(0) = \prod_{j\in N_2(i)}(1-\rho_j) = \prod_j\left(1-A_{ij}^2\rho_j\right).$$

(11)

Substituting equations (7)–(11) into equation (6), we have

$$\begin{aligned} R_{\text{inf}} = &\frac{\lambda}{2}\sum_j\left(A_{ij}^1+A_{ij}^2\right)\rho_j - \frac{\lambda}{2}\prod_j\left(1-A_{ij}^2\rho_j\right)\sum_j A_{ij}^1\left(1-A_{ij}^2\right)\rho_j \\ &-\frac{\lambda}{2}\prod_j\left(1-A_{ij}^1\rho_j\right)\sum_j A_{ij}^2\left(1-A_{ij}^1\right)\rho_j. \end{aligned}$$

(12)

Thus, the time-evolution of ρ_i can be written as

$$\frac{\mathrm{d}\rho_i}{\mathrm{d}t} = -\mu\rho_i + (1-\rho_i)R_{\text{inf}}.$$

(13)

Equation (13) is the main theoretical result of the present work. It is not hard to check that $\rho_i = 0$ $(i = 1,\cdots,N)$ is always a set of stationary solution of equation (13). Near the onset of epidemic outbreak, $\rho_i \simeq 0$, equation (13) can be linearized as,

$$\frac{\mathrm{d}\rho_i}{\mathrm{d}t} = -\mu\rho_i + \lambda\sum_j A_{ij}^1 A_{ij}^2\rho_j,$$

(14)

or in the matrix form,

$$\frac{\mathrm{d}\vec{\rho}}{\mathrm{d}t} = \left(-\mu\mathbf{I} + \lambda\tilde{\mathbf{A}}\right)\vec{\rho},$$

(15)

where $\vec{\rho} = [\rho_1,\ldots,\rho_N]^T$, $\mathbf{I}$ is the N-dimensional identity matrix, and the entries of $\tilde{\mathbf{A}}$ are $\tilde{A}_{ij} = A_{ij}^1 A_{ij}^2$. That is to say, $\tilde{A}_{ij} = 1$ only when $A_{ij}^1 = 1$ and $A_{ij}^2 = 1$ simultaneously, and therefore we call $\tilde{\mathbf{A}}$ the overlapping adjacency matrix of multiplex network. The solution $\rho_i = 0$ loses its stability when the largest eigenvalue of $-\mu\mathbf{I} + \lambda\tilde{\mathbf{A}}$ is larger than zero, which determines the epidemic threshold that is the reciprocal of the largest eigenvalue of $\tilde{\mathbf{A}}$, i.e.
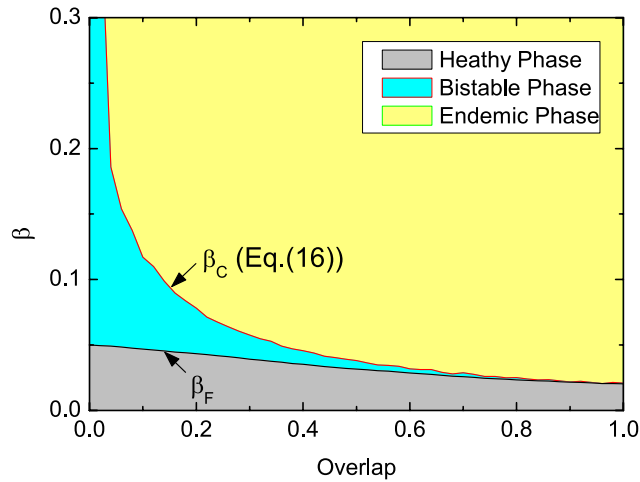
Figure 6. Phase diagram in $\beta \sim \mathcal{O}$ plane. The used networks are the same as those in figure 3.

$$\beta_C = \frac{1}{\Lambda_{\max}\left(\tilde{\mathbf{A}}\right)}. \tag{16}$$

For $\mathcal{O} = 1$, equation (16) recovers to the result of single-layer networks [68–70], $\beta_C(\mathcal{O} = 1) = 1/\Lambda_{\max}(\mathbf{A})$. For $\mathcal{O} = 0$, $\tilde{\mathbf{A}}$ becomes a null matrix and therefore $\beta_C(\mathcal{O} = 0) = \infty$. For $0 < \mathcal{O} < 1$, β_C falls between $\beta_C(\mathcal{O} = 1)$ and $\beta_C(\mathcal{O} = 0)$.

In figure 6, we show the phase diagram of the model in $\beta \sim \mathcal{O}$ space. We use the same networks as the figure 3. The phase diagram is divided into three regions, separated by two transition values of β, β_F and β_C. β_C is obtained by calculating the largest eigenvalue of the overlapping adjacency matrix (see equation (16)). Note that due to nonlinear characteristic of equation (13) β_F cannot be obtained in general by analytical derivation. Alternatively, β_F is obtained by numerically solving the steady equation of ρ_i (letting $d\rho_i/dt = 0$ in equation (13)) using the initial condition $\rho_i(0) = 1$.

4.2. Homogeneous mean-field theory

For homogeneous networks, each node is assumed to be statistically equivalent, and thus $\rho_i = \rho$ for $\forall i$, and degrees of each node in each layer are the same, i.e. $\sum_j A_{ij}^1 = \langle k \rangle_1$ and $\sum_j A_{ij}^2 = \langle k \rangle_2$ for $\forall i$. Here, the rate equation for homogeneous mean-field theory does not need to be rederived. Alternatively, it can be obtained by rewriting equation (13) based on the above assumption in homogeneous networks. Thus, $\sum_j A_{ij}^{1(2)} \rho_j = \langle k \rangle_{1(2)} \rho$, $\prod_j \left(1 - A_{ij}^{1(2)} \rho_j\right) = (1 - \rho)^{\langle k \rangle_{1(2)}}$, and $\sum_j A_{ij}^{1(2)} \left(1 - A_{ij}^{2(1)}\right) \rho_j = \langle k \rangle_{1(2)} \left(1 - \mathcal{O}_{1(2)}\right) \rho$, and equation (13) can be rewritten as,

$$\frac{d\rho}{dt} = -\mu\rho + \frac{\lambda}{2}\rho\left(1 - \rho\right)\left[\langle k \rangle_1 + \langle k \rangle_2 - \langle k \rangle_1(1 - \rho)^{\langle k \rangle_2}\left(1 - \mathcal{O}_1\right) - \langle k \rangle_2(1 - \rho)^{\langle k \rangle_1}\left(1 - \mathcal{O}_2\right)\right], \tag{17}$$

where we have defined $\mathcal{O}_{1(2)} = \sum_{i<j} A_{ij}^1 A_{ij}^2 / \sum_{i<j} A_{ij}^{1(2)}$ as the fraction of the number of overlapping edges in the total number of edges in the first (second) layer. When
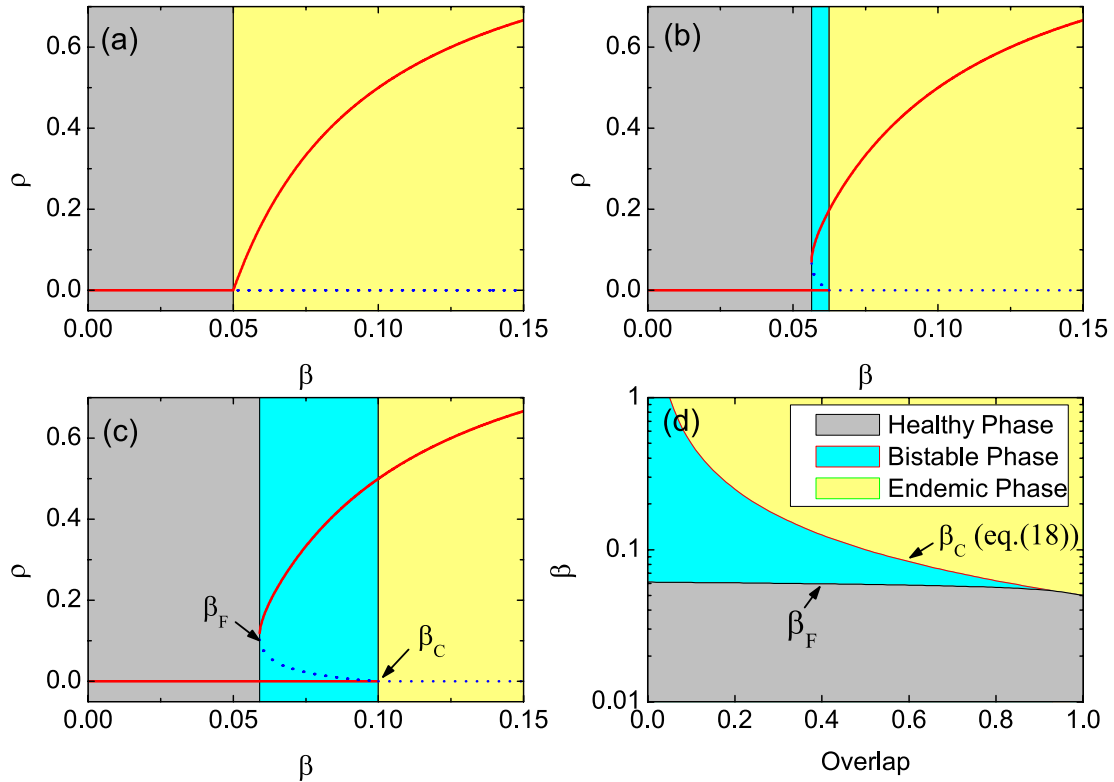
Figure 7. Results from the homogeneous mean-field theory. (a)–(c) shows ρ versus β for three different $\mathcal{O}$: 1.0 (a), 0.8 (b), and 0.5 (c). (d) Shows the phase diagram in $\beta \sim \mathcal{O}$ plane. Solid lines and dotted lines in (a)–(c) denote stable and unstable solutions, respectively. The average degree is $\langle k \rangle = 20$.

the numbers of edges in each layer are the same as considered before, $\mathcal{O}_1 = \mathcal{O}_2 = \mathcal{O}$, $\langle k \rangle_1 = \langle k \rangle_2 = \langle k \rangle$, equation (17) can be simplified to

$$\frac{\mathrm{d}\rho}{\mathrm{d}t} = -\mu\rho + \lambda \langle k \rangle (1 - \rho) \rho \left[1 - (1 - \mathcal{O})(1 - \rho)^{\langle k \rangle} \right]. \tag{18}$$

Notice that $\rho = 0$ is always a stationary solution of equation (18). Such a trivial solution corresponds to the healthy phase where no infected nodes survive. According to linear stability analysis, the solution becomes unstable when the derivative of the right-hand side of equation (18) with respect to ρ at $\rho = 0$ is larger than zero, which determines the epidemic threshold β_C,

$$\beta_C = \frac{1}{\langle k \rangle \, \mathcal{O}}. \tag{19}$$

Comparing to mean-field equation of the SIS model in single-layer networks [5], our model can give rise to an additional term in equation (18), $(1 - \mathcal{O})(1 - \rho)^{\langle k \rangle}$. Obviously, the additional term vanishes in the case of $\mathcal{O} = 1$. Importantly, we shall see that for $\mathcal{O} \neq 1$ the additional term can lead to an essential change in the bifurcation of the model. The results for the simple mean-field theory are summarized in figure 7. Figures 7(a)–(c) shows ρ as a function of β for three distinct values of $\mathcal{O}$. For $\mathcal{O} = 1$,
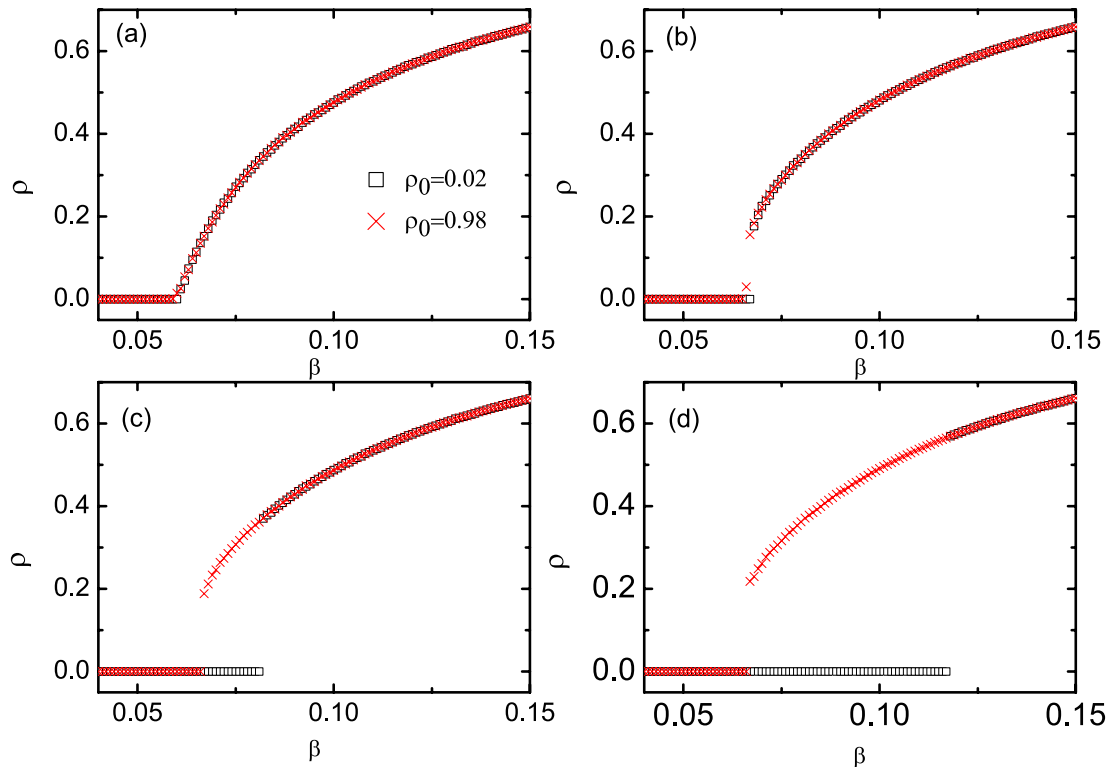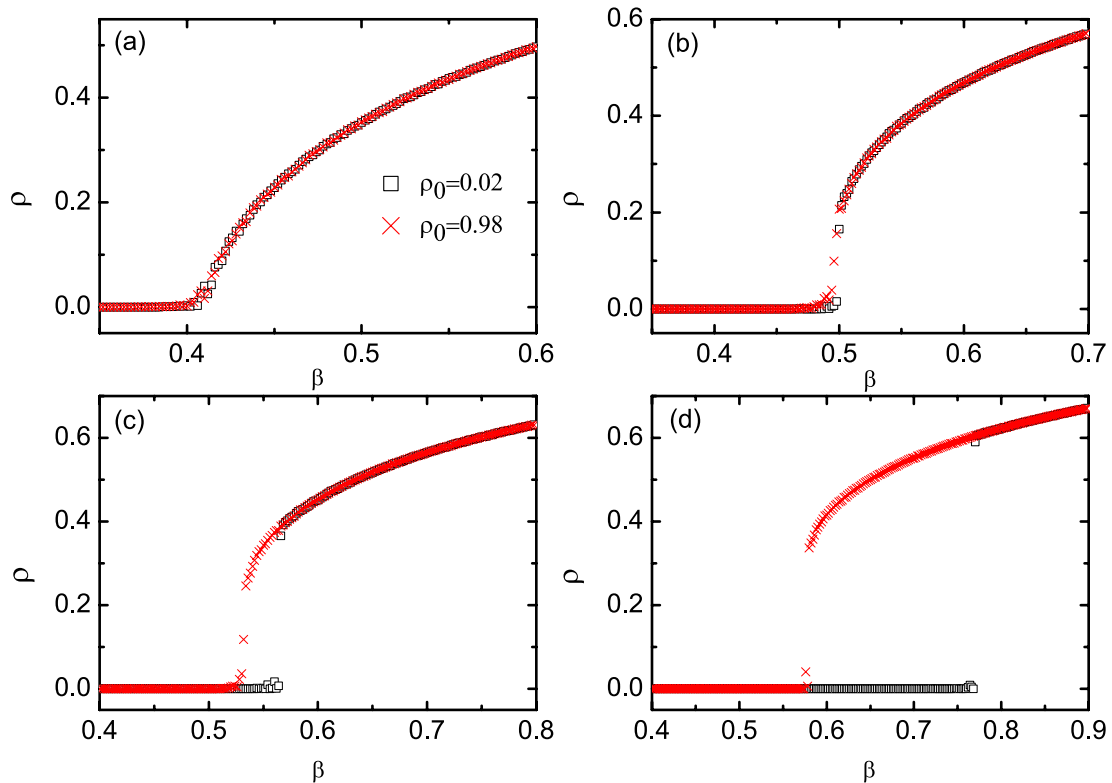
Figure 8. The density of infected nodes ρ as a function of the infection rate β in a two-layer network where the first layer is consisted of a Watts–Strogatz small-world network and the second layer is obtained by randomly rewiring the first layer network such that a given fraction of overlapping edges is achieved. Two different initial infected densities are used: $\rho_0 = 0.02$ (squares) and $\rho_0 = 0.98$ (crosses). From (a) to (d) the overlap parameters $\mathcal{O}$ are 1.0, 0.8, 0.5, and 0.2, respectively. The other parameters are $N = 10\,000$ and $\langle k \rangle = 20$.

our model recovers to the standard SIS model, and it is well-known that ρ shows a transcritical bifurcation as β varies. Across the epidemic threshold $\beta = 1/\langle k \rangle$ (here we have used $\langle k \rangle = 20$) from below, the trivial solution $\rho = 0$ loses its stability, and a new solution of $\rho \neq 0$ arises. In physics, we call that the model undergoes a continuous phase transition from a healthy phase ($\rho = 0$) to an endemic phase ($\rho > 0$) at $\beta = \beta_C$. For $\mathcal{O} \neq 1$, the bifurcation feature is changed essentially. When $\beta < \beta_F$, $\rho = 0$ is only stable solution. When $\beta_F < \beta < \beta_C$, two stable solutions exist, $\rho = 0$ and $\rho > 0$, and an unstable solution (ρ^{uns}) lying in between the two stable solutions. Depending on the initial density ρ_0 of infected nodes, the system will arrive at either a healthy phase (for $\rho_0 < \rho^{\mathrm{uns}}$) or an endemic phase (for $\rho_0 > \rho^{\mathrm{uns}}$). As β approaches β_F or β_C, one of stable solutions and the unstable solution of ρ get close to each other, until they colloid and annihilate via a saddle-node bifurcation. When $\beta > \beta_C$, $\rho = 0$ is unstable and $\rho > 0$ is only stable. Therefore, for $\mathcal{O} < 1$ the system is divided into three phases in terms of β. For $\beta < \beta_F$ the system is in the healthy phase. For $\beta > \beta_C$ the system is in the endemic phase. Between them, the system is in bistable phase. Figure 7(d) shows the phase diagram in the parametric space $\beta \sim \mathcal{O}$. The boundary line β_F shows a very slow decrease as $\mathcal{O}$ increase, and the other one β_C decreases obviously with $\mathcal{O}$ according to
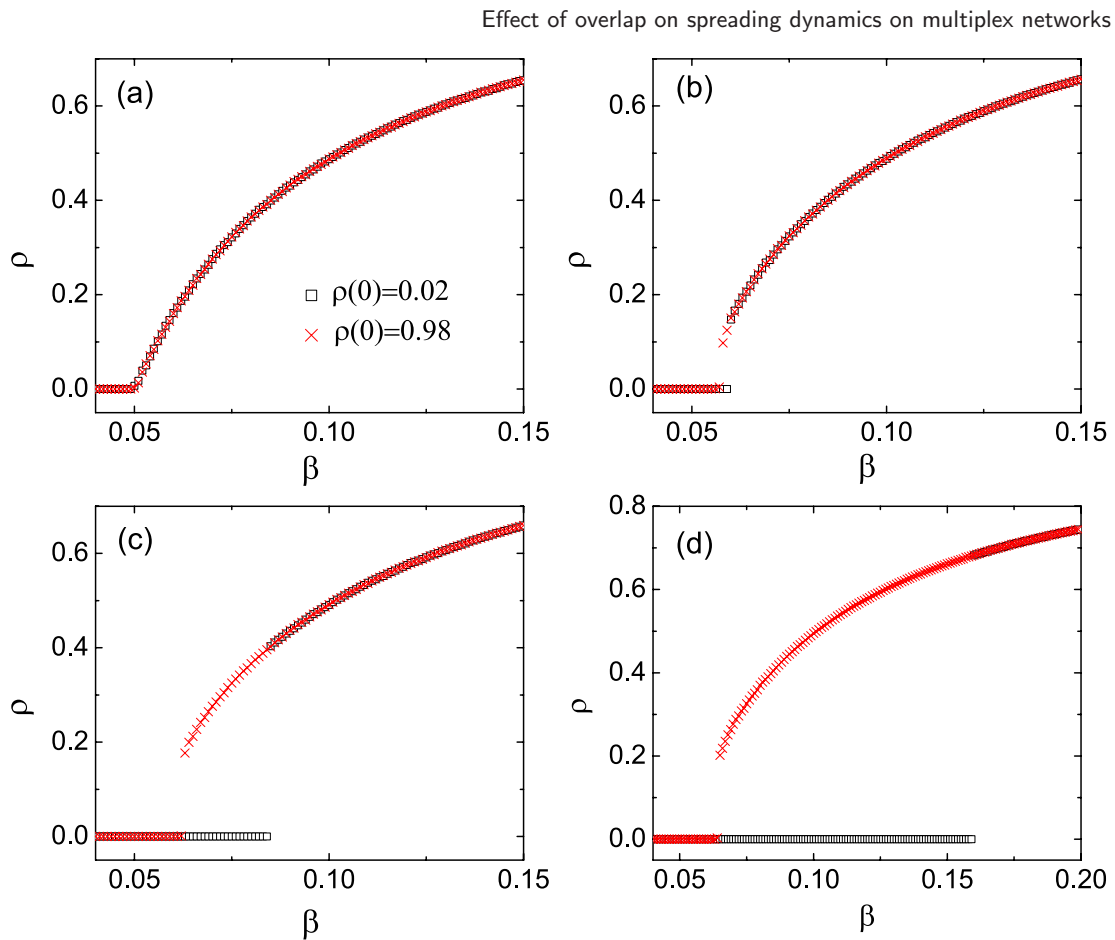
Figure 9. The density of infected nodes ρ as a function of the infection rate β in a two-layer network where the first layer is consisted of a 100×100 square lattice and the second layer is obtained by randomly rewiring the first layer network such that a given fraction of overlapping edges is achieved. Two different initial infected densities are used: $\rho_0 = 0.02$ (squares) and $\rho_0 = 0.98$ (crosses). From (a) to (d) the overlap parameters $\mathcal{O}$ are 1.0, 0.8, 0.7, and 0.5, respectively.

equation (19), such that we can see that the bistable region is clearly enlarged as $\mathcal{O}$ decreases.

5. Comparison between simulation and theory

It is expected that the homogenous mean-field theory coincides with the simulation results in the Poisson random graph (shown in figure 2). To compare them, we numerically solve equation (18) using the same initial conditions as the simulations, and theoretical results are shown by lines in figure 2. There is an excellent agreement between the theory and simulation. We should note that the theoretical value of β_C is not easy to access in simulation. For example, for $\langle k \rangle = 20$ and $\mathcal{O} = 0.5$, we have $\beta_C = 0.1$ in terms of equation (19) (shown in figure 7(c)). In simulation, we use $\rho_0 = 0.02$ and give $\beta_C = 0.076$, as shown in figure 2(c). In principle, we can access the theoretical limit of equation (19) by using a lower initial density of infection in simulation. However, if the number of infected seeds is very small, the finite-size fluctuations may drive, with a very high probability, the system to the absorbing state whenever no more infected nodes
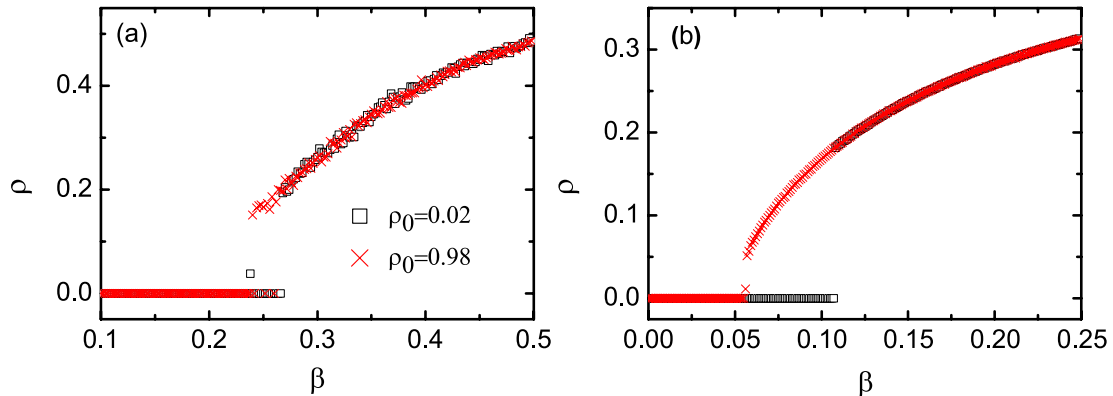
Figure 10. The density of infected nodes ρ as a function of the infection rate β in a three-layer network consisted of three Poisson random graphs. Two different initial infection densities are used: $\rho_0 = 0.02$ (squares) and $\rho_0 = 0.98$ (crosses). From (a) to (d) the overlap parameter $\mathcal{O}$ are 1.0, 0.8, 0.5, and 0.2, respectively. The other parameters are $N = 10\,000$ and $\langle k \rangle = 20$.

survive. Once the absorbing state is reached, the system cannot be left. Therefore, in order to verify the theoretical prediction in equation (19) with an adequate accuracy, one needs to use a considerable large network size to reduce the finite-size fluctuations. It will certainly increase a more computational resource.

For more degree heterogeneous networks, individual-based mean-field theory is more appropriate. Using the duplex networks the same as those in figure 3, we numerically solve equation (13) to obtain stationary value of ρ_i and the average infection density $\rho = N^{-1} \sum_{i=1}^{N} \rho_i$, as indicated by lines in figure 3. As expected, the theory can well reproduce the simulation results.

6. Results on other multiplex networks

To validate the generality of our conclusion, we also present the simulation results in other multiplex networks. In figure 8, the first layer is consisted a Watts–Strogatz

Figure 11. The density of infected nodes ρ as a function of the infection rate β in two real multiplex networks. Two different initial infection densities are used: $\rho_0 = 0.02$ (squares) and $\rho_0 = 0.98$ (crosses). (a) Elegans multiplex connectome consisted of three layers corresponding to different synaptic junctions: electric, chemical monadic, and chemical polyadic [72, 73]. The multiplex network contains 279 nodes and 5863 edges. The overlap parameter is $\mathcal{O} = 0.165$. (b) SACCHCERE multiplex network [74, 75]. The original network consisted of seven layers, but we only used the first four layers: physical association, suppressive genetic interaction defined by inequality, direct interaction, and synthetic genetic interaction defined by inequality. The multiplex network contains 6570 nodes and 151 991 edges. The overlap parameter is $\mathcal{O} = 0.013$. Note here that the number of edges in each layer is not the same, and the overlap parameter $\mathcal{O}$ is defined as the number of overlapping edges in all layers divided by the minimum of the number of edges in all layers.

small-world network [71]. The small-world network is generated as follows. We start with a regular ring network with $N = 10\,000$ nodes in which each node is connected to its first $K = 20$ neighbors ($K/2$ on either side), and we then randomly rewire each edge of the ring network with probability $p = 0.05$ such that $pNK/2$ long-range edges are generated. In figure 9, the first layer consisted of a 100×100 square lattice (periodic boundary) in which each node is connected to its four nearest neighbors. The second layers both in figures 8 and 9 are obtained by randomly rewiring the first layer network such that a given fraction of overlapping edges is achieved. From figures 8 and 9, one sees that for less degrees of overlapping edges in the two layers, a discontinuous phase transition can be also observed. That is to say, the main conclusion in our work holds for other network models as well.

In figure 10, we show the results on a three-layer network consisted of three Poisson random graphs with $N = 10\,000$ and $\langle k \rangle = 20$, in which we have assumed that a susceptible node can be infected only when it has at least one infectious neighbor in each layer. It can be seen that the main conclusions are consistent with those in a two-layer network. At last, we perform simulations on two real multiplex networks: Elegans multiplex connectome [72, 73] and SACCHCERE multiplex network [74, 75]. We find that they can produce discontinuous phase transition as well, as shown in figure 11.

7. Conclusions

In conclusion, we have studied an SIS-type epidemic spreading model in multiplex networks, in which a susceptible individual can be infected only when (s)he has at least one infectious neighbor in each layer. We find that the proportion of overlapping edges between different layers has a significant impact on the nature of phase transition for the epidemic outbreak. When all the edges are completely overlapped, the model recovers to the standard SIS model in single-layer networks, and it undergoes a continuous phase transition. Otherwise, the model shows an essentially different nature of phase transition, that is of a discontinuous first order. Using low and high initial densities of infected individuals, the model shows two distinct transition pathways from an endemic extinction phase to an endemic spread phase as the infection rate increases. Two such pathways form a hysteresis region in which the system is bistable with the coexisting endemic extinction phase and endemic spread phase. As the degree of overlapping edges decreases, the left boundary of the hysteresis region changes slowly, but the right boundary of the hysteresis region moves swiftly to a larger value of the infection rate, such that the hysteresis region is enlarged as $\mathcal{O}$ decreases. Moreover, we have developed an individual-based mean-field theory that can derive the time-evolution equations of infected probabilities of individuals. The individual-based mean-field equations can be reduced to a single equation of average infection density. Such a coarse graining is advantageous to unveil the physical mechanics of phenomena observed in simulations. By linear stability analysis, we have derived the threshold of epidemic outbreak, corresponding to the right boundary of hysteresis region. Our theory can well reproduce the simulation results.

Recently, there were some studies that reported distinct mechanisms leading to discontinuous or explosive spreading outbreak in single-layer networks, such as reinfections in social contagions [76], synergistic effect in transmission rate [77], cooperative coinfections of multiple diseases [78–80], core contact process [60, 61], and higher-order interactions between individuals [81], etc. The present work shows a new mechanism that can lead to a discontinuous phase transition due to the interacting spreading dynamics across different network layers. This mechanism underlies the importance of correlations in edges belong to different layers. Therefore, our study adds to the continuing effort of the effects of multiplexity on dynamic processes on multiplex networks, compared to conventional single-layer ones. On the one hand, in most social systems, individuals interact with each other in complicated patterns that include multiple types of relationships. The present findings may improve our understanding for some real-world spreading processes in such complex systems such as the spread of a rumor, the formation of a new opinion. On the other hand, a common characteristic of discontinuous epidemic outbreak is that infinitesimal increase of the external parameters, such as infection rate, can give rise to a considerable macroscopic spreading scope. There is no doubt that it brings more challenges for controlling or predicting epidemic outbreaks [82]. Finally, we expect that the present theoretical findings can be supported by empirical or experimental research in the future.

Acknowledgments

References

[1] Newman M 2018 *Networks* (Oxford: Oxford University Press)
[2] Newman M E J 2003 *SIAM Rev.* **45** 167
[3] Boccaletti S, Latora V, Moreno Y, Chavez M and Hwang D-U 2006 *Phys. Rep.* **424** 175
[4] Arenas A, Díaz-Guilera A, Kurths J, Moreno Y and Zhou C 2008 *Phys. Rep.* **469** 93
[5] Pastor-Satorras R, Castellano C, Van Mieghem P and Vespignani A 2015 *Rev. Mod. Phys.* **87** 925
[6] Perc M, Jordan J J, Rand D G, Wang Z, Boccaletti S and Szolnoki A 2017 *Phys. Rep.* **687** 1
[7] Dorogovtsev S N, Goltseve A V and Mendes J F F 2008 *Rev. Mod. Phys.* **80** 1275
[8] Kivelä M, Arenas A, Barthelemy M, Gleeson J P, Moreno Y and Porter M A 2014 *J. Complex Netw.* **2** 203
[9] Bianconi G 2018 *Multilayer Networks: Strcuture and Function* (Oxford: Oxford University Press)
[10] Boccaletti S, Bianconi G, Criado R, del Genio C, Gómez-Gardeñes J, Romance M, Sendiña-Nadal I, Wang Z and Zanin M 2014 *Phys. Rep.* **544** 1
[11] Buldyrev S V, Parshani R, Paul G, Stanley H E and Havlin S 2010 *Nature* **464** 1025
[12] Baxter G J, Dorogovtsev S N, Goltsev A V and Mendes J F F 2012 *Phys. Rev. Lett.* **109** 248701
[13] Gómez S, Díaz-Guilera A, Gómez-Gardeñes J, Pérez-Vicente C J, Moreno Y and Arenas A 2013 *Phys. Rev. Lett.* **110** 028701
[14] Radicchi F and Arenas A 2013 *Nat. Phys.* **9** 717
[15] Wang Z, Wang L, Szolnoki A and Perc M 2015 *Eur. Phys. J.* B **88** 124
[16] Battiston F, Perc M and Latora V 2017 *New J. Phys.* **19** 073017
[17] Xia C, Li X, Wang Z and Perc M 2018 *New J. Phys.* **20** 075005
[18] Aguirre J, Sevilla-Escoboza R, Gutiérrez R, Papo D and Buldú J M 2014 *Phys. Rev. Lett.* **112** 248701
[19] Majhi S, Perc M and Ghosh D 2016 *Sci. Rep.* **6** 39033
[20] del Genio C I, Gómez-Gardeñes J, Bonamassa I and Boccaletti S 2016 *Sci. Adv.* **2** e1601679
[21] Diakonova M, San Miguel M and Eguíluz V M 2014 *Phys. Rev.* E **89** 062818
[22] Diakonova M, Nicosia V, Latora V and Miguel M S 2016 *New J. Phys.* **18** 023010
[23] Solé-Ribalta A, Gómez S and Arenas A 2016 *Phys. Rev. Lett.* **116** 108701
[24] Manfredi S, Di Tucci E and Latora V 2018 *Phys. Rev. Lett.* **120** 068301
[25] Solé-Ribalta A, De Domenico M, Kouvaris N E, Díaz-Guilera A, Gómez S and Arenas A 2013 *Phys. Rev.* E **88** 032807
[26] Cencetti G and Battiston F 2019 *New J. Phys.* **21** 035006
[27] Hinrichsen H 2000 *Adv. Phys.* **49** 815
[28] Vespignani A 2012 *Nat. Phys.* **8** 32
[29] Salehi M, Sharma R, Marzolla M, Magnani M, Siyari P and Montesi D 2015 *IEEE Trans. Netw. Sci. Eng.* **2** 65
[30] Domenico M D, Granell C, Porter M A and Arenas A 2016 *Nat. Phys.* **2** 901
[31] de Arruda G F, Rodrigues F A and Moreno Y 2018 *Phys. Rep.* **756** 1
[32] Cozzo E, Baños R A, Meloni S and Moreno Y 2013 *Phys. Rev.* E **88** 050801
[33] Wang H, Li Q, D'Agostino G, Havlin S, Stanley H E and Van Mieghem P 2013 *Phys. Rev.* E **88** 022801
[34] Saumell-Mendiola A, Serrano M A and Boguñá M 2012 *Phys. Rev.* E **86** 026106
[35] Dickison M, Havlin S and Stanley H E 2012 *Phys. Rev.* E **85** 066109
[36] Bianconi G 2017 *J. Stat. Mech.* 034001
[37] Soriano-Paños D, Lotero L, Arenas A and Gómez-Gardeñes J 2018 *Phys. Rev.* X **8** 031039
[38] Xuan Q, Du F, Yu L and Chen G 2013 *Phys. Rev.* E **87** 032809
[39] Wang B, Tanaka G, Suzuki H and Aihara K 2014 *Phys. Rev.* E **90** 032806
[40] de Arruda G F, Cozzo E, Peixoto T P, Rodrigues F A and Moreno Y 2017 *Phys. Rev.* X **7** 011014
[41] De Domenico M, Solé-Ribalta A, Cozzo E, Kivelä M, Moreno Y, Porter M A, Gómez S and Arenas A 2013 *Phys. Rev.* X **3** 041022
[42] Goltsev A V, Dorogovtsev S N, Oliveira J G and Mendes J F F 2012 *Phys. Rev. Lett.* **109** 128702
[43] Nicosia V, Skardal P S, Arenas A and Latora V 2017 *Phys. Rev. Lett.* **118** 138302
[44] Zhang X, Boccaletti S, Guan S and Liu Z 2015 *Phys. Rev. Lett.* **114** 038701

[45] Granell C, Gómez S and Arenas A 2013 *Phys. Rev. Lett.* **111** 128701
[46] Kan J-Q and Zhang H-F 2017 *Commun. Nonlinear Sci.* **44** 193
[47] Wang W, Tang M, Yang H, Do Y, Lai Y-C and Lee G 2014 *Sci. Rep.* **4** 5097
[48] Mishkovski I, Mirchev M, Scepanovic S and Kocarev L 2017 *IEEE Trans. Circuits Syst.* I **64** 2761
[49] An N, Chen H, Ma C and Zhang H 2018 *New J. Phys.* **20** 125006
[50] Velásquez-Rojas F and Vazquez F 2017 *Phys. Rev.* E **95** 052315
[51] Pires M A, Oestereich A L and Crokidakis N 2018 *J. Stat. Mech.* 053407
[52] Jiang J and Zhou T 2018 *Sci. Rep.* **8** 1629
[53] Su Z, Wang W, Li L, Stanley H and Braunstein L A 2018 *New J. Phys.* **20** 053053
[54] Chen X, Wang R, Tang M, Cai S, Stanley H and Braunstein L A 2018 *New J. Phys.* **20** 013007
[55] Zhang Z-K, Liu C, Zhan X-X, Lu X, Zhang C-X and Zhang Y-C 2016 *Phys. Rep.* **651** 1
[56] Bianconi G 2013 *Phys. Rev.* E **87** 062806
[57] Jalan S and Pradhan P 2018 *Phys. Rev.* E **97** 042314
[58] Centola D 2010 *Science* **329** 1194
[59] Watts D J 2002 *Proc. Natl Acad. Sci.* **99** 5766
[60] Chae H, Yook S-H and Kim Y 2015 *New J. Phys.* **17** 023039
[61] Varghese C and Durrett R 2013 *Phys. Rev.* E **87** 062819
[62] Chowdhury D, Schadschneider A and Nishinari K 2005 *Phys. Life Rev.* **2** 318
[63] Gillespie D T 1977 *J. Phys. Chem.* **81** 2340
[64] Erdös P and Rényi A 1959 *Publ. Math.* **6** 290
[65] Barabási A-L and Albert R 1999 *Science* **286** 509
[66] Jalan S, Kumar A and Leyva I 2019 *Chaos* **29** 041102
[67] Jalan S, Rathore V, Kachhvah A D and Yadav A 2019 *Phys. Rev.* E **99** 062305
[68] Wang Y, Chakrabarti D, Wang C and Faloutsos C 2003 *22nd Int. Symp. on Reliable Distributed Systems* (IEEE Computer Society) p 25
[69] Mieghem P V, Omic J and Kooij R 2009 *IEEE ACM Trans. Netw.* **17** 1
[70] Gómez S, Arenas A, Borge-Holthoefer J, Meloni S and Moreno Y 2010 *Europhys. Lett.* **89** 38009
[71] Watts D J and Strogatz S H 1998 *Nature* **393** 440
[72] Chen B L, Hall D H and Chklovskii D B 2006 *Proc. Natl Acad. Sci.* **103** 4723
[73] De Domenico M, Porter M A and Arenas A 2015 *J. Complex Netw.* **3** 159
[74] Stark C, Breitkreutz B-J, Reguly T, Boucher L, Breitkreutz A and Tyers M 2006 *Nucleic Acids Res.* **34** D535
[75] De Domenico M, Nicosia V, Arenas A and Latora V 2015 *Nat. Commun.* **6** 6864
[76] Gómez-Gardeñes J, de Barros A S, Pinho S T and Andrade R F 2015 *Europhys. Lett.* **110** 58006
[77] Gómez-Gardeñes J, Lotero L, Taraskin S and Pérez-Reche F 2016 *Sci. Rep.* **6** 19767
[78] Chen L, Ghanbarnejad F, Cai W and Grassberger P 2013 *Europhys. Lett.* **104** 50001
[79] Cai W, Chen L, Ghanbarnejad F and Grassberger P 2015 *Nat. Phys.* **4** 2412
[80] Hébert-Dufresnea L and Althousea B M 2015 *Proc. Natl Acad. Sci. USA* **112** 10551
[81] Iacopini I, Petri G, Barrat A and Latora V 2019 *Nat. Commun.* **10** 2485
[82] D'Souza R M, Gómez-Gardeñes J, Nagler J and Arenas A 2019 *Adv. Phys.* **68** 123